
LOW-RESOLUTION FACE RECOGNITION IN RESOURCE-CONSTRAINED ENVIRONMENTS*

A PREPRINT

Mozhdeh Rouhsedaght
University of Southern California
Los Angeles, California, USA
rouhseda@usc.edu

Yifan Wang
University of Southern California
Los Angeles, California, USA
wang608@usc.edu

Shuowen Hu
Army Research Lab
Adelphi, Maryland, USA
shuowen.hu.civ@mail.mil

Suya You
Army Research Lab
Adelphi, Maryland, USA
suya.you.civ@mail.mil

C.-C. Jay Kuo
University of Southern California
Los Angeles, California, USA
jckuo@usc.edu

November 25, 2020

ABSTRACT

A non-parametric low-resolution face recognition model for resource-constrained environments with limited networking and computing is proposed in this work. Such environments often demand a small model capable of being effectively trained on a small number of labeled data samples, with low training complexity, and low-resolution input images. To address these challenges, we adopt an emerging explainable machine learning methodology called successive subspace learning (SSL). SSL offers an explainable non-parametric model that flexibly trades the model size for verification performance. Its training complexity is significantly lower since its model is trained in a one-pass feedforward manner without backpropagation. Furthermore, active learning can be conveniently incorporated to reduce the labeling cost. The effectiveness of the proposed model is demonstrated by experiments on the LFW and the CMU Multi-PIE datasets.

1 Introduction

Cloud-based face recognition has reached maturity in recent years. Deep neural network (DNN) models consisting of millions of model parameters have been developed and made significant progress. The high performance mainly relies on several factors: higher input image resolutions, using an extremely large number of training images, and abundant computational/memory resources. Take the models which have achieved high accuracy on the LFW benchmark as an example. DeepFace [1] was trained on a collection of photos from Facebook that contains 4.4M images. FaceNet [2] was trained on the Google dataset that contains 500M images. SphereFace [3] was trained on the CASIA-WebFace dataset [4] that contains 0.49M images. Along this direction, many activities are centered on face images collection and the setup of the required computing and communication environment.

We may face an opposite situation in some real-world applications; i.e., edge or mobile computing in resource-constrained environments with poor computing and communication infrastructure, as is often the case in the field and in operational settings. Such environments demand smaller model size, fewer labeled images for training, lower training and inference complexity, and lower input image resolution, partly due to the need to image individuals at farther standoff distances. Due to these stringent requirements, DNNs may not be applicable. The goal of this work is to address these challenges and develop a robust and transparent non-parametric model that allows graceful performance tradeoff between resources and performance and is capable of being easily integrated with active learning to minimize the training sample number while achieving relatively high accuracy. We adopt an emerging machine learning system

*This paper is under consideration at Pattern Recognition Letters

called PixelHop++ [5] to achieve these objectives. PixelHop++ is designed based on the successive subspace learning (SSL) principle and has several unique characteristics that fit our objectives well.

1. PixelHop++ is a light-weight non-parametric model whose size can be flexibly adjusted for graceful performance tradeoff. Its training is conducted in a feedforward one-pass manner and the training complexity is significantly lower than DNNs.
2. SSL adopts a statistics-centric principle. It exploits pixel-to-pixel correlations for dimension reduction to derive image features. It also analyzes statistics between features and labels to identify discriminant features. SSL is mathematically transparent.
3. We will incorporate active learning in SSL to select the most “informative” samples of a dataset for labeling and reduce the labeling cost. PixelHop++ is a lightweight model, and it can easily be integrated with active learning.

The main contribution of our work lie in the assembly of two effective tools to address the challenge of face recognition in resource-constrained environments. Both PixelHop++ and active learning are existing tools. Yet, to the best of our knowledge, this is the first time that they are jointly applied to a face biometric problem. We will demonstrate the power of the integrated solution in the context of face recognition with extensive experiments.

The rest of the paper is organized as follows. Related prior work is reviewed in Sec. 2. The proposed face recognition method and its integration with active learning are presented in Sec. 3 and Sec. 4, respectively. Experimental results are provided in Sec. 5. Finally, concluding remarks and future work are given in Sec. 6.

2 Related Work

Face Recognition. Face recognition has made significant progress in recent years. Most successful face recognition models use deep learning technique [1, 6, 2, 7, 3] and offer high accuracy on the benchmarking datasets. Although these models are powerful for high-resolution face recognition, they usually contain tens of millions of model parameters and require a large amount of training data and computation resources. A light-weight CNN model called Light CNN was proposed in [8] which is significantly smaller than regular CNN networks but still has millions of model parameters.

Low-Resolution Face Recognition. In comparison with high-resolution face recognition, less attention has been drawn to low-resolution face recognition. Generally, there are two different settings for this problem: high-resolution to low-resolution, and low-resolution to low-resolution. In the first setting, the low-resolution probe images are compared against high-resolution gallery images [9, 10, 11] while in the second setting both probe and gallery images are low-resolution face images [12, 13, 14]. We evaluate our model under the second setting and compare it with the model proposed in [14].

Successive Subspace Learning (SSL). The main technique in subspace learning is to project a high-dimension input space to a low-dimensional output subspace, which serves as an approximation to the original one. When these dimension reduction operations are performed sequentially, it leads to successive subspace learning (SSL). PixelHop++ [5] is a model developed using the SSL principle. It is proposed for unsupervised representation learning by applying the channel-wise (c/w) Saab transform to images. The Saab transform [15] is a multi-stage variant of principal component analysis (PCA) conducted on images. In each stage, it applies PCA to pixel blocks and also uses a bias term to avoid the sign-confusion problem [16]. The performance of the Saab transform can be further enhanced by removing the spatial correlation between Saab transform outputs in the current stage so that the Saab transform can be applied to each output channel separately in the next stage. PixelHop++ with the c/w Saab transform is proven to offer an effective multi-stage representation. For example, FaceHop [17] is recently proposed for gender classification on gray-scale face images. It uses PixelHop++ for feature learning. In this paper, besides incorporating chrominance channels of face images, we add a new module for effective pair-wise feature extraction to tackle the face recognition problem.

Active Learning. Active learning is used to select the most informative unlabeled data for labeling so that almost the same accuracy can be reached with the smallest amount of labeled data. An active learning method begins with a small amount of labeled data to train a machine learning model. The model queries the labels of some unlabeled data based on a query strategy, and the model is retrained by all labeled data. This process is repeated until we reach the labeled sample budget. Common query strategies include the entropy method [18], the query by committee method [19] and the core-set method [20]. Active learning was incorporated in DNNs by Wang *et al.* [21]. An active annotation and learning framework is introduced in [22] for the face recognition task.

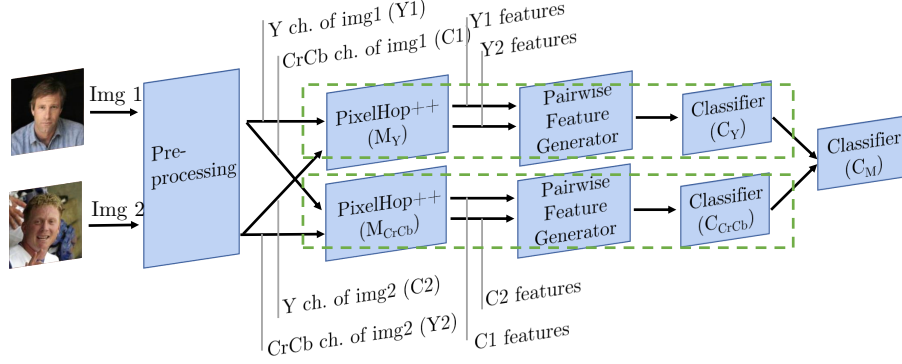


Figure 1: The block diagram of the proposed face recognition method.

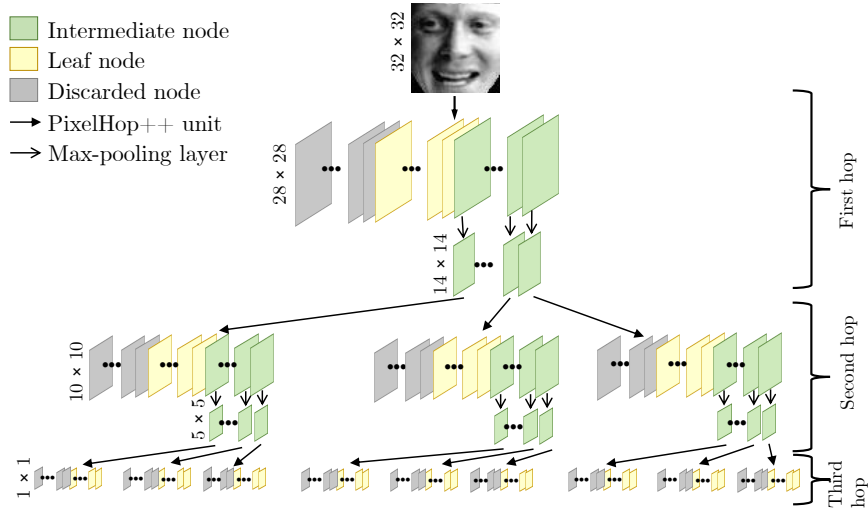


Figure 2: Illustration of data flow in the three-level c/w Saab transform in PixelHop++, which provides a sequence of successive subspace approximations (SSAs) to the input image.

3 Proposed Face Recognition Method

The block diagram of the proposed face recognition method is shown in Fig. 1. As shown in the figure, our model is an ensemble of two submodels, each of which consists of three components, i.e., PixelHop++, pairwise feature generation, and classifier. We will elaborate the function of each component of the block diagram below.

3.1 Preprocessing

Several commonly used face processing techniques are adopted in the preprocessing block such as

1. Applying a 2D face alignment algorithm to the input face images to reduce the effect of pose variation;
2. Cropping face images properly to eliminate background;
3. Using histogram equalization (HE) to reduce the effect of different illumination conditions on the Y channel.

We use the dlib [23] toolkit for face detection and landmark localization. Face images are aligned/normalized so that the line connecting the eye centers is horizontal and all faces are centered and resized into a constant size of 32x32 pixels. We convert the color space to YCrCb and, then, feed the Y channel (the luminance component) separately to one submodel and the Cr and Cb channels (chrominance components) to another submodel.

3.2 PixelHop++

In each submodel, we use a three-level PixelHop++ system, similar to the system shown in Fig. 2. The input to each of the PixelHop++ systems is a whole face image of resolution $32 \times 32 \times K_0$, where $K_0 = 1$ and 2 for the Y channel and CrCb channels, respectively. Each level of a PixelHop++ system has one PixelHop++ unit followed by (2×2) -to- (1×1) max-pooling. In our model, the PixelHop++ unit of each level operates on blocks of 5×5 pixels with a stride of one. In the training phase of each PixelHop++ unit, we collect sample blocks from each input channel to derive Saab kernels for that channel separately. Then, we project each block on the derived kernels and generate a set of responses for the central pixel in the block. Since the responses can be positive or negative, we add a constant bias to all responses to ensure that they are all non-negative, which explains the name of the ‘‘successive approximation with adjusted bias (Saab) transform’’ [15].

The first Saab kernel is the unit-length constant-element vector that computes the local mean of each block which we call the DC component. After removing the DC, we conduct PCA on residual blocks. Since each block has 25 dimensions, we get one DC component plus 24 AC components, whose kernels are eigenvectors of the covariance matrix of the collected blocks, for each channel. In each level, the corresponding Saab components of the blocks of each channel form an output channel (or a node in a tree as shown in Fig. 2), e.g. the DC component of blocks extracted from an input channel from one output channel/node. We divide these nodes into three groups:

- Intermediate nodes: The DC and several leading low-frequency AC channels will be forwarded to the next level for further energy compaction.
- Leaf nodes: The nodes which are kept at the current level.
- Discarded nodes: AC components with very small eigenvalues are discarded.

As we mentioned, in each PixelHop++ unit we apply channel-wise (c/w) transform to pixel blocks; in other words, for pixel blocks extracted from each individual input channel, an individual Saab transform is applied. The reason we can process channels individually is that all AC channels are orthogonal to the DC channel and all AC responses are uncorrelated due to PCA. Note that the first PixelHop++ unit of M_{CrCb} is an exception (Cr and Cb channels are not uncorrelated), so we apply Saab transform on blocks of $5 \times 5 \times 2$ pixels at this level and obtain 1 DC component and 49 AC components for each pixel block. We should emphasize that *channel separability* is powerful in reducing our model size and computational complexity. Unlike DNNs, PixelHop++ does not transform one large 3D (i.e., 2D spatial plus 1D spectral) tensor but multiple 2D spatial tensors.

Each level of PixelHop++ provides an approximation to the input with different spatial/frequency tradeoffs. The input is a pure spatial representation. The output of Level-3 is a pure frequency representation. The outputs of Level-1 and Level-2 are hybrid spatial/frequency representations. A square in Fig. 2 indicates a channel which is the union of all corresponding spatial locations. Before max-pooling, the dimensions of the output channels of Level-1 and Level-2 are 28×28 and 10×10 , respectively. Clearly, Level-1 has more spatial detail than Level-2. The spatial dimension of Level-3 is 1×1 . Each intermediate/leaf node at a level indicates a frequency channel at the corresponding level.

For channels at each level, we need two hyper-parameters to partition them into the mentioned three groups. We use the energy level of a channel as the criterion. If its energy is less than a cutoff energy level denoted by E_C , the channel is discarded. If its energy is higher than a forwarded energy level denoted by E_F , the channel is forwarded to the next level. We normalize the energy of the root node (i.e., the input image) to 100%. The energy level of each intermediate/leaf node is computed as follows.

- Step 1: Initial DC and AC energy computation for each PixelHop++ unit.
Each eigenvalue of the covariance matrix indicates the energy of its corresponding node. We define the initial energy (E_{init}) of each output node as the ratio of its corresponding eigenvalue to the sum of all others eigenvalues related to that PixelHop++ unit. At this step, the sum of the DC and total AC energy values for each PixelHop++ unit is 100%.
- Step 2: Normalized energy at each node.
Based on the first step, we have the energy of an intermediate/leaf node against its siblings. By traversing the tree from the root node to a leaf node, the path includes intermediate nodes. The normalized energy of a leaf node against the root node is the product of E_{init} values of all visited nodes (including itself).

Note that by lowering E_C and E_F , we can obtain a better approximation at the cost of higher model complexity.

3.3 Pairwise Feature Generation

To compare whether two face images are similar or not, we can examine their similarities at different spatial regions, channels, and levels. This is feasible because of the rich representations offered by PixelHop++. Note that although

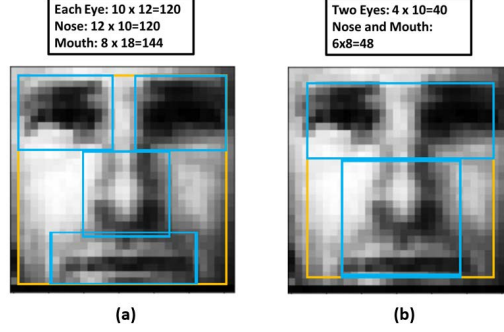


Figure 3: Illustration of selected spatial regions of interest (ROIs) with respect to the input image for frequency channels at (a) Level-1 and (b) Level-2.

the content of an intermediate node will be mainly forwarded to the next level, it does have different spatial/spectral representations at two adjacent levels. Thus, for feature extraction, we do not differentiate intermediate/leaf nodes at each level.

There are K_1 , K_2 and K_3 nodes at Level-1, Level-2 and Level-3, respectively, as shown in Fig. 2. We can process them individually as detailed below.

- **Level-1.** It has the highest spatial resolution 28×28 . We can use it to zoom in on salient regions of the face such as the left eye, the right eye, the nose, and the mouth of certain dimensions at each channel (see Fig. 3(a)) and flatten them to form vectors. Accordingly, we extract 4 feature vectors from each node at this level ($4 \times K_1$ feature vectors).
- **Level-2.** It has a lower spatial resolution (10×10). We can still zoom in on unions of salient regions such as one horizontal stripe covering two eyes and one vertical stripe covering the nose and the mouth at each channel (see Fig. 3(b)) and form 2 vectors per node accordingly ($2 \times K_2$ feature vectors).
- **Level-3.** It has no spatial resolution. Each leaf node offers a scalar description of the whole face. In our implementation, we concatenate all K_3 nodes into a long sequence and then group every 10 nodes as one vector. Consequently, we obtain P feature vectors, where P is the floor of K_3 divided by 10.

To compare the similarity between two face images, we collect corresponding vector pairs from the same spatial region of the same node (including intermediate and leaf nodes) at each level and compute two similarity measures for them - the cosine similarity (C_k) and the length ratio (R_k) for the k -th vector pair. We define the length ratio of two vectors as the ratio of the vector with smaller L2 norm to the vector with larger L2 norm. If two images are similar, their cosine similarity and length ratio should be close to unity. Otherwise, they should be farther away from (and less than) one. We observe experimentally that an individual R_k value is not as discriminant as C_k . Instead, the average length ratio for each spatial region in Level-1 and -2 as shown in Fig. 3 and the average length ratio for P pairs in Level-3 is more robust and discriminant.

To summarize, the ultimate feature vector to be fed to the binary classifier is the concatenation of: 1) 7 average length ratio values (4 extracted from Level-1, 2 from Level-2, and 1 from Level-3), 2) $4 \times K_1$ cosine similarity values from four spatial regions and K_1 channels, 3) $2 \times K_2$ cosine similarity values from two spatial regions and K_2 channels, and 4) P cosine similarity values from groups of channels in Level-3. The value of the feature dimension (N) for each submodel is given in Table. 1.

3.4 Classifiers

As described in Sec. 3.3, we extract the feature vector from the Y channel and the CrCb channels of each pair separately. For each pairwise feature, we train a classifier which makes a soft decision, i.e., the probability for the pair to be match or mismatch. Then, we feed these two probabilities into a meta classifier for the final decision. We use the LR classifier in our experiments to achieve a smaller model size although using larger binary classifiers we may achieve higher accuracy.

4 Integration with Active Learning

The feature generation process in our model is unsupervised, and labels are only needed for classifier training. As a motivation for active learning, a scenario of interest is training a model on a mobile agent when the model has access to unlabeled training samples locally but has to fetch the label of a limited number of samples from the server through unreliable low-bandwidth channels. To overcome the communication constraint, active learning can be used to retrieve labels of most informative samples. We consider three active learning methods as explained below.

1. *Entropy method*: In each iteration, compute the entropy of each sample in the pool of unlabeled data D^u and pick the samples with higher entropy to add to the labeled training data. Higher entropy means the model is more uncertain about those samples. The entropy for sample x can be computed using

$$\text{entropy}(x) = - \sum_{j=1}^J p(y_j | x) \log p(y_j | x), \quad (1)$$

where $p(y_i | x)$ is the probability that sample x belongs to the class label y_i .

2. *Query By Committee (QBC)*: Instead of training one model, this method trains several models called a committee. In each iteration, measure the disagreement between the committee members for each sample in the pool of unlabeled data and pick the ones with the largest disagreement values. One of the common disagreement measures is Vote Entropy which can be computed using

$$VE(x) = - \sum_{j=1}^J \frac{V(y_j)}{C} \log \frac{V(y_j)}{C}, \quad (2)$$

where C is the number of models, $V(y_i)$ is the number of votes which label y_i receives from committee members.

3. *Core-set method*: The core-set selection problem is choosing b sample points from the pool of unlabeled data that minimize the maximum distance between each data point remaining in the pool and its nearest data point in the selected subset. This problem is NP-Hard. A greedy approach for core-set selection is the k-Center-Greedy algorithm. In the i^{th} iteration, it selects the samples from D^u with the maximum distance from their closest sample in the labeled training data D_{i-1}^l .

5 Experiments

We evaluate the performance of the proposed method by conducting experiments on two well-known datasets: Labeled Faces in the Wild (LFW) [24] and CMU Multi-PIE [25]. In all the experiments, we use low-resolution face images of size 32×32 unless otherwise specified.

The *LFW dataset* is a widely used dataset for face verification. It consists of 13,233 face images of 5,749 individuals. For performance benchmarking of different face verification models, it provides 6,000 face pairs in 10 splits. We follow the "Image-Restricted, Label-Free Outside Data" protocol. We choose this protocol as we use a tool for facial landmark localization in the preprocessing step. But for training the model, we only use face images in the LFW training set. A 3D aligned version of LFW [26] is used in experiments. For data augmentation, we add the pair of horizontally flipped images of each training pair to the training data.

The *CMU Multi-PIE dataset* contains more than 750,000 images of 337 people recorded in four sessions. For each identity, images are captured under 15 viewpoints and 19 illumination conditions with a few different facial expressions. In experiments, we select a subset of 01 session which contains frontal and slightly non-frontal face images (camera views 05_0, 05_1, and 14_0) with a neutral expression and under all existing illumination conditions.

5.1 Face Verification on LFW

Experiment #1. We use the first 90% of the LFW training pairs for training the model and the rest of the pairs for testing. The parameters of each PixelHop++ model and the accuracy of the classifiers trained on their output features are given in Table. 1. We set $E_C = E_F$ so that the number of leaf nodes in the first and second hop is zero. The test accuracy of the meta classifier (C_M) under this setting is 85.33%. We use the same hyper-parameters in all experiments.

Experiment #2. To compare our model with the state-of-the-art, we compute the 10-fold cross-validation accuracy for the input resolution of 32×32 and 16×16 . To obtain the 16×16 face images, we down-sample images to 16×16

Table 1: Comparison of test accuracy of C_Y and C_{CrCb} and hyper-parameter settings of M_Y and M_{CrCb} , where K_1 , K_2 , and K_3 are numbers of intermediate and leaf nodes at Level-1, Level-2, and Level-3, P is the number of vectors at Level-3 and $N = 7 + 4K_1 + 2K_2 + P$ is the feature dimension.

| Input ch. | E_C | K_1 | K_2 | K_3 | P | N | Acc. |
|-----------|--------|-------|-------|-------|-----|-----|-------|
| Y | 0.0005 | 18 | 119 | 233 | 23 | 340 | 83.47 |
| CrCb | 0.0004 | 19 | 73 | 124 | 12 | 241 | 75.89 |

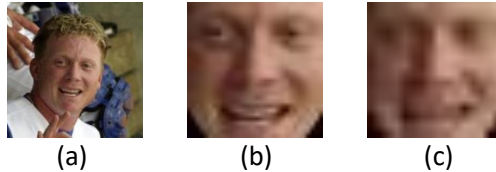


Figure 4: Quality of the obtained 32×32 (b) and 16×16 (c) low-resolution face images compared with the original high-resolution face image (a).

and then resize them back to 32×32. The quality of the obtained face images is compared in Fig. 4. To the best of our knowledge, there is no low-resolution to low-resolution face recognition model which has reported accuracy under the “Image-Restricted, Label-Free Outside Data” protocol on LFW. To this end, we compare our model with the SKD (Selective Knowledge Distillation) model [14] which is a recent state-of-the-art model for low-resolution face recognition using unlimited training data.

We have compared our model, SKD without distillation, and SKD in terms of accuracy, the number of parameters, and the number of training images for each input resolution in Table. 2. We see that for 16×16 image resolution our model achieves an accuracy of 82.16% which is only 3.71% lower than SKD, and for 32×32 image resolution our model achieves an accuracy of 83.49% which is only 6.42% lower than SKD while in both cases, our model size is about 79× smaller and uses only 5400 pair of images as the training set. On the other hand, SKD uses a pre-trained model on the VGGFace dataset [7] with 2.6 M images as its teacher model and train and fine-tunes its student model on the UMDFaces dataset [27] with 367,888 images. Based on these results, our model does have a competitive performance for deployment in resource-constrained environments.

Experiment #3. In this experiment, we use the three active learning methods which are introduced in Sec. 4 to obtain the minimum required number of labeled training pairs without significant loss in recognition accuracy. We use the first 90% of the LFW training pairs as the initial pool of unlabeled data (D_u) and the rest as the test data, then we randomly select 5% of the pool as D_0 . The data augmentation step is removed. For the QBC algorithm, we use two different classifiers (LR and SVM) as the committee of classifiers. We apply each active learning algorithm to samples and compute the test accuracy versus the number of labeled training pairs used for training the model. The result is shown in Fig. 5.

By comparing the performance of different algorithms, we see that QBC is the most effective one for our model in the current experiment setting as it has the fastest convergence in test accuracy and also the most stable performance. For example, with this algorithm, our model can achieve an accuracy of above 84% using only 1465 training pairs. Furthermore, our model achieves a stable accuracy of about 86% with only 3000 pairs.

Table 2: Low-Resolution Face verification results on LFW.

| Model | Resolution | #Param. | training set (#Img.) | Acc.(%) |
|--------------------------|------------|---------|-------------------------------------|---------|
| SKD without distillation | 16×16 | 0.79 M | UMDFaces (367,888) | 62.82 |
| SKD | 16×16 | 0.79 M | VGGFace (2.6 M), UMDFaces (367,888) | 85.87 |
| Ours | 16×16 | 0.01 M | LFW (5400 pairs) | 82.16 |
| SKD without distillation | 32×32 | 0.79 M | UMDFaces (367,888) | 70.23 |
| SKD | 32×32 | 0.79 M | VGGFace (2.6 M), UMDFaces (367,888) | 89.72 |
| Ours | 32×32 | 0.01 M | LFW(5400 pairs) | 83.30 |

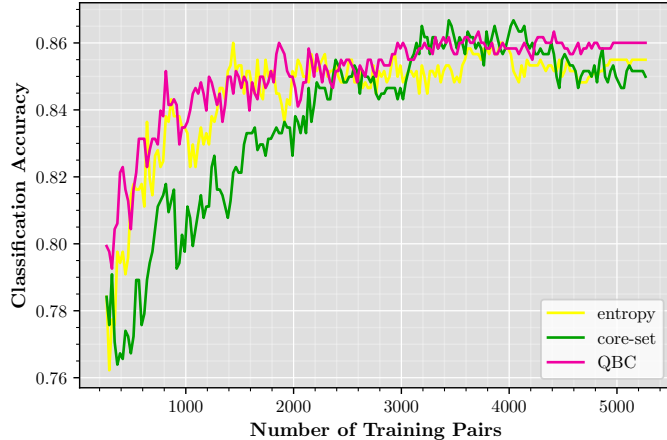


Figure 5: Comparison of classification accuracy of three active learning methods as a function of the number of training pairs.

Table 3: Rank-1 identification rate (%) for frontal and slightly non-frontal face images ($\pm 15^\circ$) in Setting-1.

| Method | Resolution | Acc.(%) |
|-------------------|------------|---------|
| CPF [28] | 60×60 | 89.45 |
| HPN [29] | 256×220 | 84.23 |
| c-CNN Forest [30] | - | 96.97 |
| Light CNN-29 [8] | 128×128 | 99.78 |
| TP-GAN [31] | 128×128 | 99.78 |
| Ours | 32×32 | 89.48 |

5.2 Face Identification on CMU Multi-PIE

We evaluate the effectiveness of our model for the face identification task by conducting experiment on the Multi-PIE dataset. To the best of our knowledge, no low-resolution face recognition model has reported results on this dataset. Thus, we compare our model with high-resolution face recognition models that have used this dataset for performance benchmarking. We use a setting mentioned in [28] as Setting-1. According to this setting, the first 150 identities are used for training and the rest of the identities (151-250) from session 01 with neutral expression are used for test so that there is no overlap between training and test identities. As the gallery image, one frontal face image with frontal illumination is used and the rest of the images in the test set are selected as probes. For model training, we generate 17,888 training pairs by pairing probe images with gallery images and 21,000 training pairs by randomly pairing images with each other. Overall, 38,888 training pairs are used to train our model.

Since our model is not proposed for handling pose variation, we report results only for frontal and slightly non-frontal images ($\pm 15^\circ$) in the dataset. The rank-1 face identification accuracy is shown in Table. 3. Our model has competitive and comparable performance although it uses low-resolution face images and a small training set and has a small model size. For example, Light CNN-29 has 12.637M parameters and uses 128×128 images while our model size is 1,149× smaller and uses 32×32 images. It is worthwhile to comment that TP-GAN in Table. 3 also uses Light CNN-29 for feature extraction from images so its model is larger than Light CNN-29.

5.3 Model size computation

We compute the size of our model based on the information in Table 1. Each of the two PixelHop++ systems in our model has three levels and the *c/w* Saab transform is applied on 5×5 blocks with a stride of one in each level. Since $E_C = E_F$, there are no leaf nodes in the first and second levels. The first level of the M_Y system has 18 intermediate nodes and 7 discarded nodes (25-18). Thus, it has 25×18 variables for storing PCA components and one bias parameter (451 parameters in total). The second level has 119 intermediate nodes and 25×18-119 discarded nodes. For each of the 18 output channels of level one, the Saab transform is applied separately. Initially, 25×18 nodes are generated, and 119 of them are then selected as intermediate nodes based on the energy threshold. For each Saab transform, the DC

Table 4: The number of the parameters for different components of our model

| subsystem | Num. of Param. |
|----------------------------|----------------|
| First hop - M_Y | 451 |
| Second hop - M_Y | 2,543 |
| Third hop - M_Y | 2,969 |
| Pairwise Feat. Gen. - Y | 740 |
| LR Classifier - C_Y | 341 |
| First hop - M_{CrCb} | 476 |
| Second hop - M_{CrCb} | 1,369 |
| Third hop - M_{CrCb} | 1,348 |
| Pairwise Feat. Gen. - CrCb | 432 |
| LR Classifier - C_{CrCb} | 242 |
| Meta Classifier | 3 |
| Total | 10,914 |

kernel is known and constant so we have 18 repetitive kernels in the second level. As a result, we have $25 \times (119 - 18)$ parameters for storing PCA components and 18 bias parameters which is in total 2,543 parameters. By the same token, there are $25 \times (233 - 119) + 199$ parameters in the third level of M_Y . In the Pairwise Feature Generator - Y unit, the mean and the standard deviation of each PixelHop++ output node is stored. Hence, the size of the unit is $2 \times (18 + 119 + 233)$ equal to 740. The LR classifier’s size equals its input feature size plus one which is 341 for C_Y . Likewise, the size of all subsystems is computed and summarized in Table. 4.

6 Conclusion and Future Work

A non-parametric solution targeting low-resolution face recognition for resource-constrained environments was proposed in this work. Face biometric attributes (e.g., gender, ethnicity, age, etc.) prediction could be explored using a similar methodology. Furthermore, the advantages of our solution may not be limited to resource-constrained environments. The same SSL principle could be generalized to resource-rich environments and high-resolution images. They are all interesting topics for future research.

7 Acknowledgements

This work was sponsored by US Army Research Office (ARO) under contract number W911NF1820218 through Carnegie Mellon University under subaward number 1130234-421349.

References

- [1] Yaniv Taigman, Ming Yang, Marc’Aurelio Ranzato, and Lior Wolf. Deepface: Closing the gap to human-level performance in face verification. In *Proceedings of the IEEE conference on computer vision and pattern recognition*, pages 1701–1708, 2014.
- [2] Florian Schroff, Dmitry Kalenichenko, and James Philbin. Facenet: A unified embedding for face recognition and clustering. In *Proceedings of the IEEE conference on computer vision and pattern recognition*, pages 815–823, 2015.
- [3] Weiyang Liu, Yandong Wen, Zhiding Yu, Ming Li, Bhiksha Raj, and Le Song. Spheroface: Deep hypersphere embedding for face recognition. In *Proceedings of the IEEE conference on computer vision and pattern recognition*, pages 212–220, 2017.
- [4] Dong Yi, Zhen Lei, Shengcai Liao, and Stan Z Li. Learning face representation from scratch. *arXiv preprint arXiv:1411.7923*, 2014.
- [5] Yueru Chen, Mozhdah Rouhsedaghat, Suya You, Raghuveer Rao, and C-C Jay Kuo. Pixelhop++: A small successive-subspace-learning-based (ssl-based) model for image classification. *arXiv preprint arXiv:2002.03141*, 2020.
- [6] Yi Sun, Yuheng Chen, Xiaogang Wang, and Xiaoou Tang. Deep learning face representation by joint identification-verification. In *Advances in neural information processing systems*, pages 1988–1996, 2014.

- [7] Omkar M Parkhi, Andrea Vedaldi, and Andrew Zisserman. Deep face recognition. 2015.
- [8] Xiang Wu, Ran He, Zhenan Sun, and Tieniu Tan. A light cnn for deep face representation with noisy labels. *IEEE Transactions on Information Forensics and Security*, 13(11):2884–2896, 2018.
- [9] Soma Biswas, Kevin W Bowyer, and Patrick J Flynn. Multidimensional scaling for matching low-resolution face images. *IEEE transactions on pattern analysis and machine intelligence*, 34(10):2019–2030, 2011.
- [10] Sivaram Prasad Mudunuri and Soma Biswas. Low resolution face recognition across variations in pose and illumination. *IEEE transactions on pattern analysis and machine intelligence*, 38(5):1034–1040, 2015.
- [11] Ze Lu, Xudong Jiang, and Alex Kot. Deep coupled resnet for low-resolution face recognition. *IEEE Signal Processing Letters*, 25(4):526–530, 2018.
- [12] Zhangyang Wang, Shiyu Chang, Yingzhen Yang, Ding Liu, and Thomas S Huang. Studying very low resolution recognition using deep networks. In *Proceedings of the IEEE Conference on Computer Vision and Pattern Recognition*, pages 4792–4800, 2016.
- [13] Zhiyi Cheng, Xiatian Zhu, and Shaogang Gong. Low-resolution face recognition. In *Asian Conference on Computer Vision*, pages 605–621. Springer, 2018.
- [14] Shiming Ge, Shengwei Zhao, Chenyu Li, and Jia Li. Low-resolution face recognition in the wild via selective knowledge distillation. *IEEE Transactions on Image Processing*, 28(4):2051–2062, 2018.
- [15] C-C Jay Kuo, Min Zhang, Siyang Li, Jiali Duan, and Yueru Chen. Interpretable convolutional neural networks via feedforward design. *Journal of Visual Communication and Image Representation*, 60:346–359, 2019.
- [16] C.-C. Jay Kuo. Understanding convolutional neural networks with a mathematical model. *Journal of Visual Communication and Image Representation*, 41:406–413, 2016.
- [17] Mozhddeh Rouhsedaghat, Yifan Wang, Xiou Ge, Shuowen Hu, Suyu You, and C-C Jay Kuo. Facehop: A light-weight low-resolution face gender classification method. *arXiv preprint arXiv:2007.09510*, 2020.
- [18] Claude E Shannon. A mathematical theory of communication. *Bell system technical journal*, 27(3):379–423, 1948.
- [19] H Sebastian Seung, Manfred Opper, and Haim Sompolinsky. Query by committee. In *Proceedings of the fifth annual workshop on Computational learning theory*, pages 287–294, 1992.
- [20] Ozan Sener and Silvio Savarese. Active learning for convolutional neural networks: A core-set approach. *arXiv preprint arXiv:1708.00489*, 2017.
- [21] Keze Wang, Dongyu Zhang, Ya Li, Ruimao Zhang, and Liang Lin. Cost-effective active learning for deep image classification. *IEEE Transactions on Circuits and Systems for Video Technology*, 27(12):2591–2600, 2016.
- [22] Hao Ye, Weiyan Shao, Hong Wang, Jianqi Ma, Li Wang, Yingbin Zheng, and Xiangyang Xue. Face recognition via active annotation and learning. In *Proceedings of the 24th ACM international conference on Multimedia*, pages 1058–1062, 2016.
- [23] Davis E. King. Dlib-ml: A machine learning toolkit. *Journal of Machine Learning Research*, 10:1755–1758, 2009.
- [24] Gary B Huang, Marwan Mattar, Tamara Berg, and Eric Learned-Miller. Labeled faces in the wild: A database for studying face recognition in unconstrained environments. 2008.
- [25] Ralph Gross, Iain Matthews, Jeffrey Cohn, Takeo Kanade, and Simon Baker. Multi-pie. *Image and Vision Computing*, 28(5):807–813, 2010.
- [26] Claudio Ferrari, Giuseppe Lisanti, Stefano Berretti, and Alberto Del Bimbo. Effective 3d based frontalization for unconstrained face recognition. In *2016 23rd International Conference on Pattern Recognition (ICPR)*, pages 1047–1052. IEEE, 2016.
- [27] Ankan Bansal, Anirudh Nanduri, Carlos D Castillo, Rajeev Ranjan, and Rama Chellappa. Umdfaces: An annotated face dataset for training deep networks. In *2017 IEEE International Joint Conference on Biometrics (IJCB)*, pages 464–473. IEEE, 2017.
- [28] Junho Yim, Heechul Jung, ByungIn Yoo, Changkyu Choi, Dusik Park, and Junmo Kim. Rotating your face using multi-task deep neural network. In *Proceedings of the IEEE Conference on Computer Vision and Pattern Recognition*, pages 676–684, 2015.
- [29] Changxing Ding and Dacheng Tao. Pose-invariant face recognition with homography-based normalization. *Pattern Recognition*, 66:144–152, 2017.

- [30] Chao Xiong, Xiaowei Zhao, Danhang Tang, Karlekar Jayashree, Shuicheng Yan, and Tae-Kyun Kim. Conditional convolutional neural network for modality-aware face recognition. In *Proceedings of the IEEE International Conference on Computer Vision*, pages 3667–3675, 2015.
- [31] Rui Huang, Shu Zhang, Tianyu Li, and Ran He. Beyond face rotation: Global and local perception gan for photorealistic and identity preserving frontal view synthesis. In *Proceedings of the IEEE International Conference on Computer Vision*, pages 2439–2448, 2017.